Supporting Information for

Ultrasensitive Dual-mode Visualization of Perchlorate in Water, Soil and Air Boosted by Close and Stable Pt-Pt Packing Endowed Low-energy Absorption and Emission

Zhen Su,[ab] Yushu Li,*[a] Jiguang Li,[ab] Kun Li,*[c] and Xincun Dou*[ab]

[a] Xinjiang Key Laboratory of Explosives Safety Science, Xinjiang Technical Institute of Physics & Chemistry; Key Laboratory of Functional Materials and Devices for Special Environments, Chinese Academy of Sciences, Urumqi 830011, China

[b] Center of Materials Science and Optoelectronics Engineering, University of Chinese Academy of Sciences, Beijing 100049, China

[c] Shanxi Key Laboratory of Metal Forming Theory and Technology, School of Material Science and Engineering, Taiyuan University of Science and Technology, Taiyuan 030024, China.

* Corresponding authors. E-mail: liys@ms.xjb.ac.cn (Yushu Li); likun@tyust.edu.cn (Kun Li); xcdou@ms.xjb.ac.cn (Xincun Dou)

Supplementary Figures

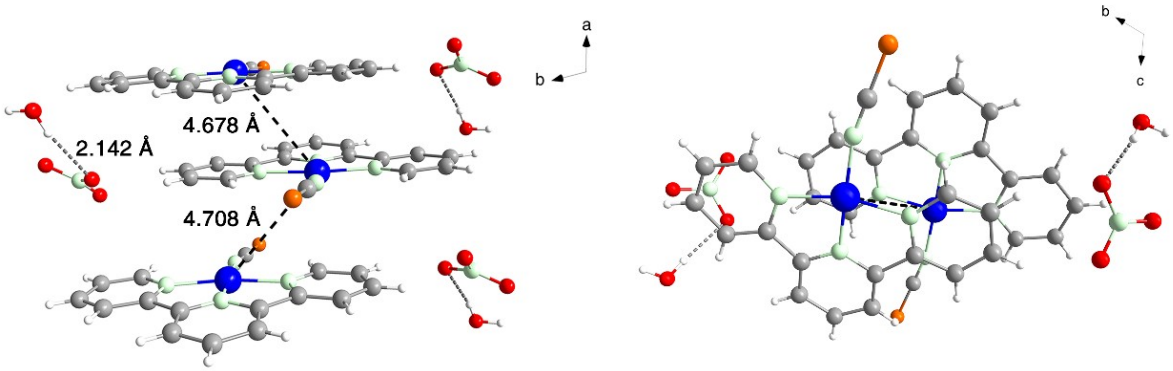

Fig. S1. Single crystal structure of [Pt(tpy)NCS]·NO_3·H_2O from side view (left) and top view (right).

Discussion: As determined by X-ray crystallography, its crystal structure belongs to *P-1* space group, with 1D columnar stack of planar molecules extending parallel to the crystallographic *a*-axis. Due to the hydrophilicity, NO_3^- bonds a solvated water-molecule through H-bonds (bond length for HO-H···ONO_2^- is 2.142 Å). Adjacent Pt-centers adopt a zig-zag arrangement with a Pt-Pt-Pt angle of 103.36°. Individual molecules are rotated with respect to their neighbors, with a (SCN)-Pt-Pt-(NCS) torsion angle of 180.00° and almost no stacking of the aromatic terpyridyl units. Stacked Pt atoms are separated by an alternate Pt-Pt distance of 4.678/4.708 Å, indicating the absence of metal-metal interaction.

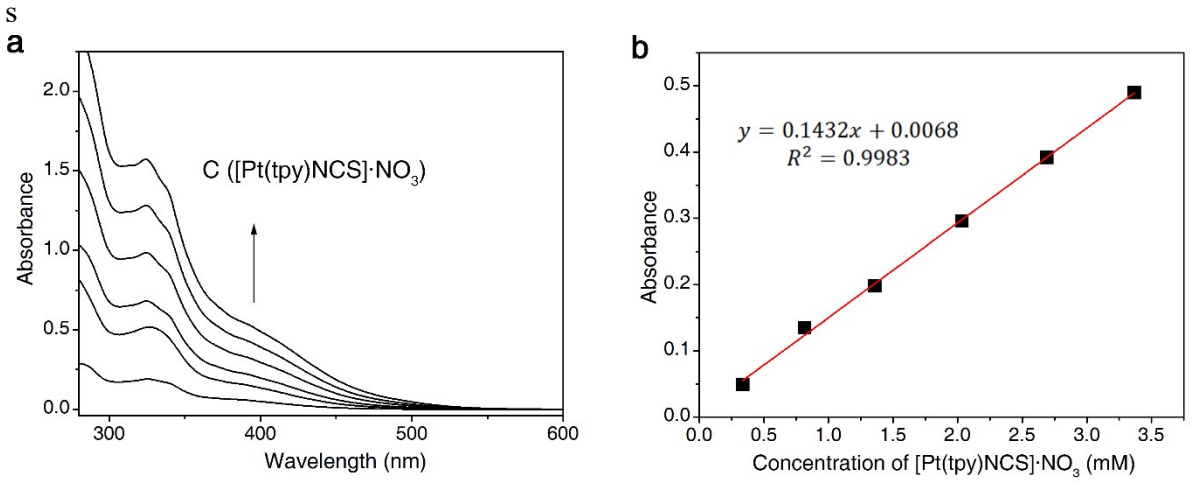

Fig. S2. a) UV-vis absorption spectra of [Pt(tpy)NCS]·NO_3 aqueous solution in the concentration range of 0.3 mM to 3.5 mM, tested with the optical path length of 1 mm. b) The linear fitting of absorbance at 400 nm as a function of [Pt(tpy)NCS]·NO_3 concentration.

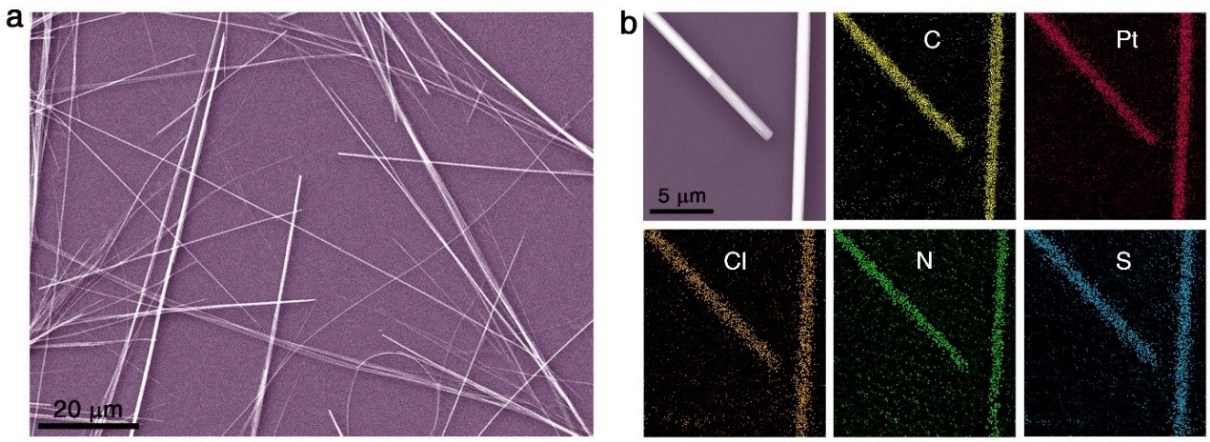

Fig. S3. a) SEM image of generated 1D aggregates of [Pt(terpy)NCS]·ClO_4·H_2O. b) EDS mapping of the 1D aggregates.

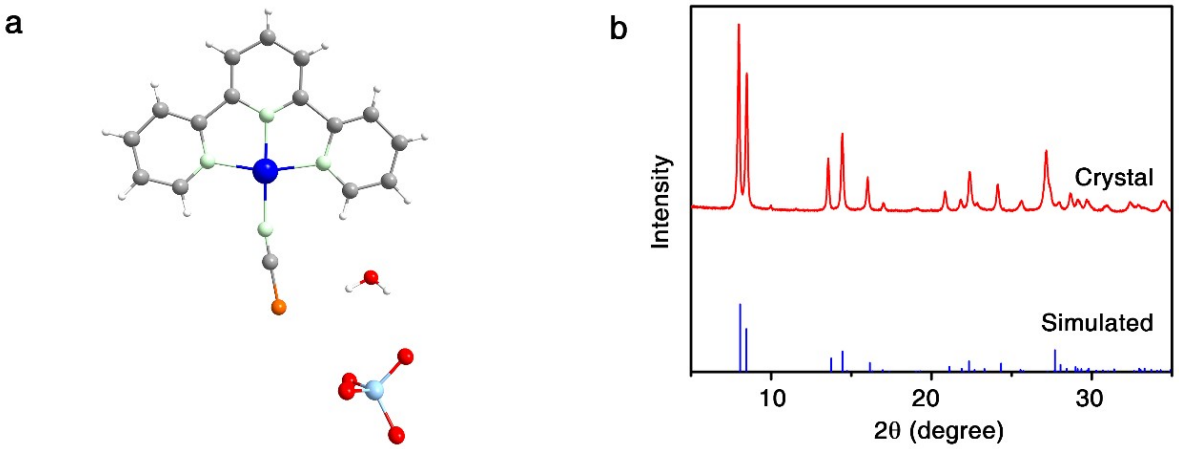

Fig. S4. a) Atomic arrangement in the asymmetric unit of the hydrated single-crystal structure of [Pt(tpy)NCS]·ClO_4·H_2O. b) Simulated XPRD pattern with the experimental pattern of powdered sample.

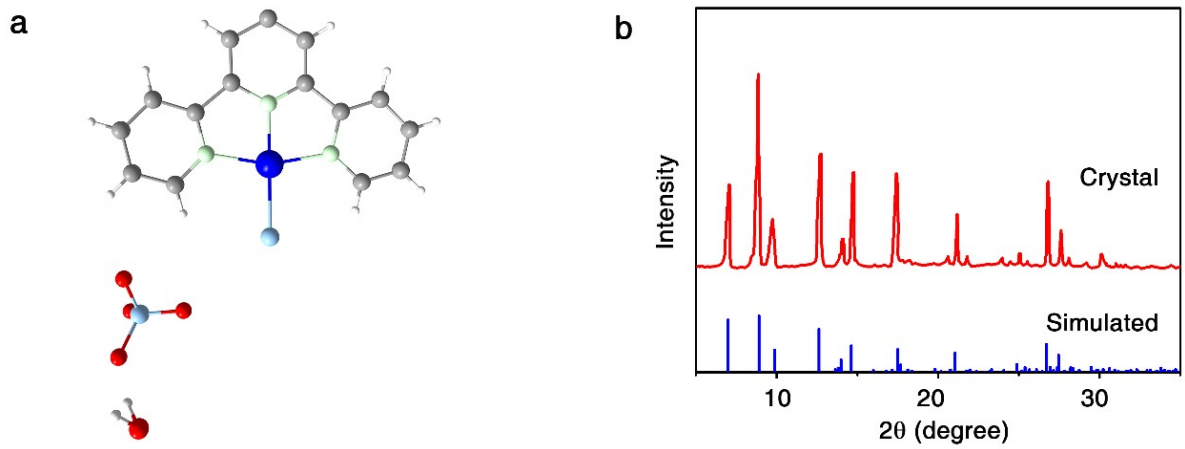

Fig. S5. a) Atomic arrangement in the asymmetric unit of the hydrated single-crystal structure of [Pt(tpy)Cl]·ClO_4·H_2O. b) Simulated XPRD pattern with the experimental pattern of powdered sample.

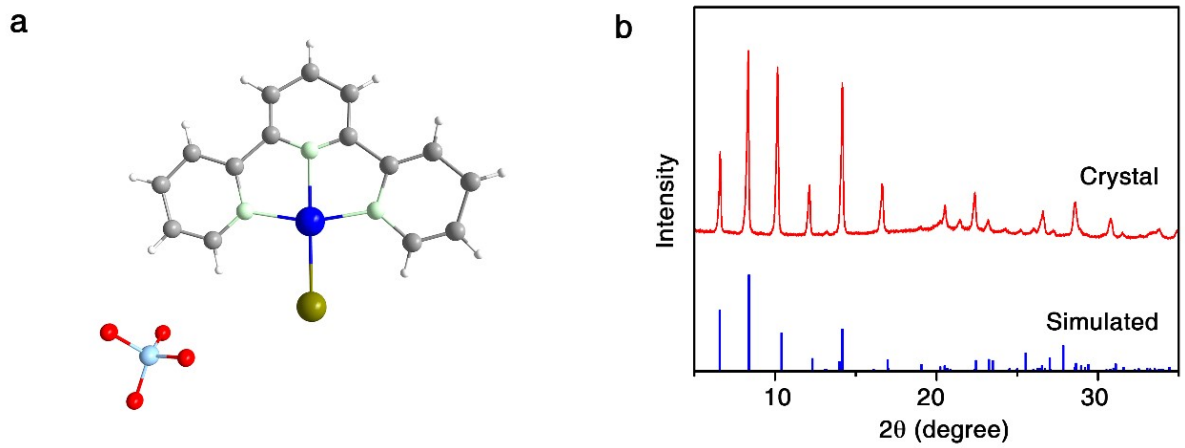

Fig. S6. a) Atomic arrangement in the asymmetric unit of the single-crystal structure of [Pt(tpy)I]·ClO_4. b) Simulated XPRD pattern with the experimental pattern of powdered sample.

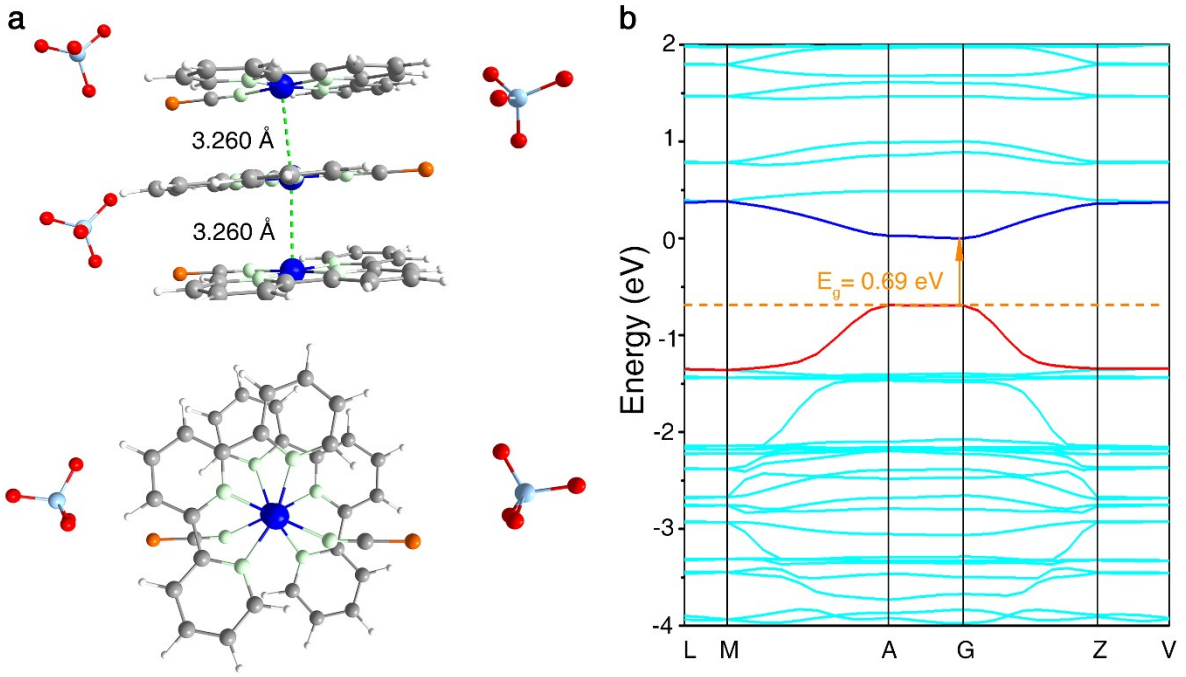

Fig. S7. a) Simulated crystal structure of dehydrated compund of [Pt(tpy)NCS]·ClO_4. b) Calculated band structure for the structure of [Pt(tpy)NCS]·ClO_4.

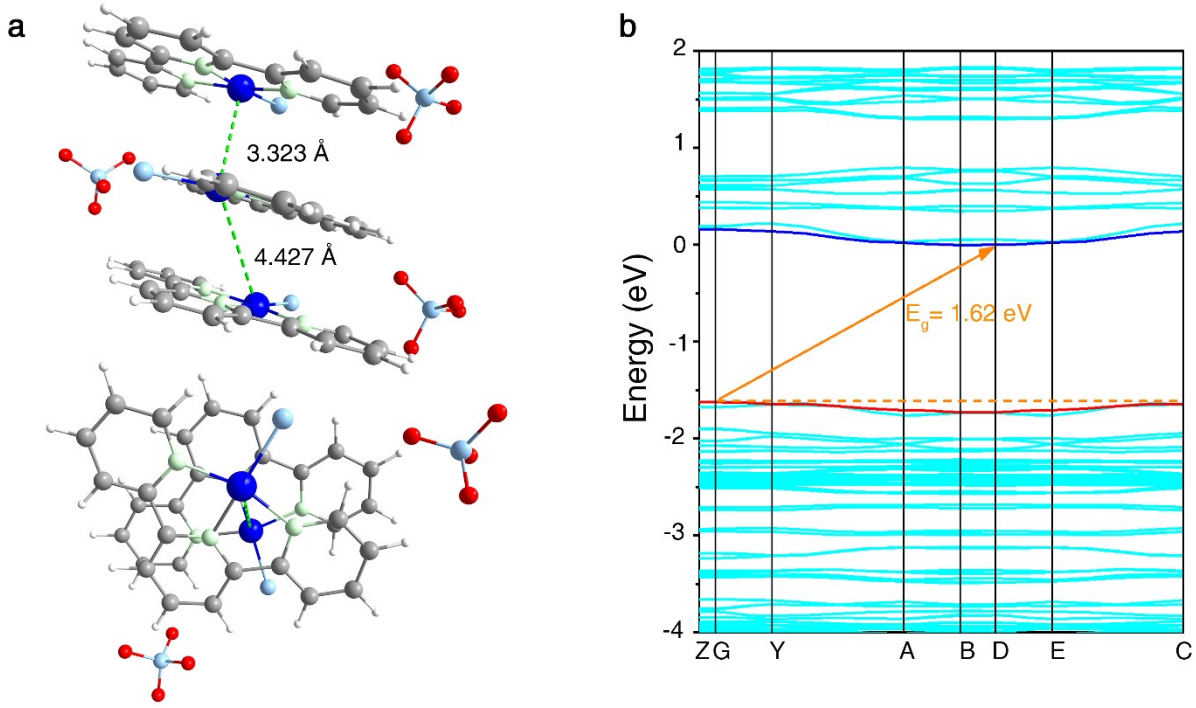

Fig. S8. a) Simulated crystal structure of dehydrated compund of [Pt(tpy)Cl]·ClO_4. b) Calculated band structure for the structure of [Pt(tpy)Cl]·ClO_4.

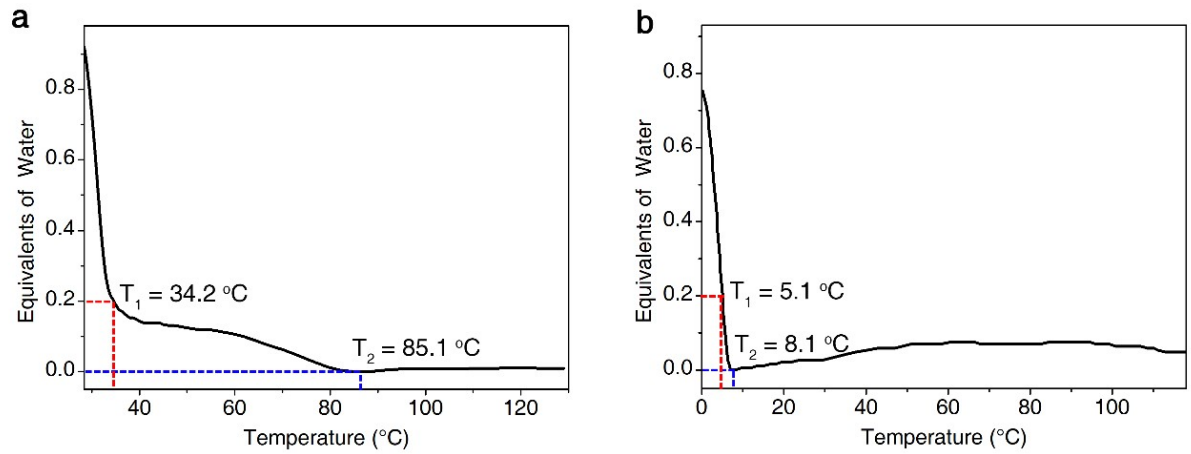

Fig. S9. a) Thermogravimetric analysis for $[Pt(tpy)NCS]\cdot ClO_4\cdot H_2O$ at the heating rate as low as 1 °C min^{-1}. b) Thermogravimetric analysis for $[Pt(tpy)Cl]\cdot ClO_4\cdot H_2O$ at the heating rate as low as 1 °C min^{-1}, reported by previous study.[1]

Discussion: As shown in Fig. S9, the loss of crystal water in complex $[Pt(tpy)NCS]\cdot ClO_4\cdot H_2O$ is much slower than in $[Pt(tpy)Cl]\cdot ClO_4\cdot H_2O$ compound. For $[Pt(tpy)NCS]\cdot ClO_4\cdot H_2O$, the temperatures corresponding to 0.2 and 0 equivalents of water are 34.2 °C and 85.1 °C, respectively. As comparison, for $[Pt(tpy)Cl]\cdot ClO_4\cdot H_2O$, the temperatures corresponding to 0.2 and 0 equivalents of water are much lower (5.1 °C and 8.1 °C, respectively). This indicates that the solvated water molecule in $[Pt(tpy)Cl]\cdot ClO_4\cdot H_2O$ is less stable than that in $[Pt(tpy)NCS]\cdot ClO_4\cdot H_2O$.

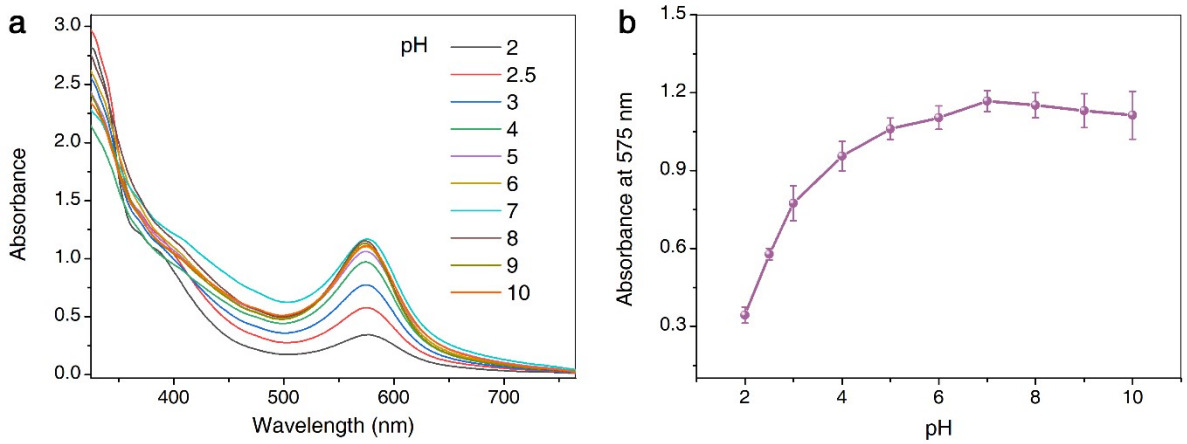

Fig. S10. a) UV-vis absorption changes at different initial pH of $[Pt(tpy)NCS]\cdot NO_3$ aqueous solution (0.6 mM) after adding perchlorate (0.5 mM). b) Corresponding absorbance at 575 nm under different pH.

Discussion: As shown in Fig. S10, the characteristic absorption peak at 575 nm gradually enhanced with initial pH value raising from 2 to 6, which then increased little with further raise of pH, demonstrating that the neutral or alkaline environment is conductive to the formation of $[Pt(tpy)NCS]\cdot ClO_4\cdot H_2O$ aggregate and thus beneficial to the sensing application.

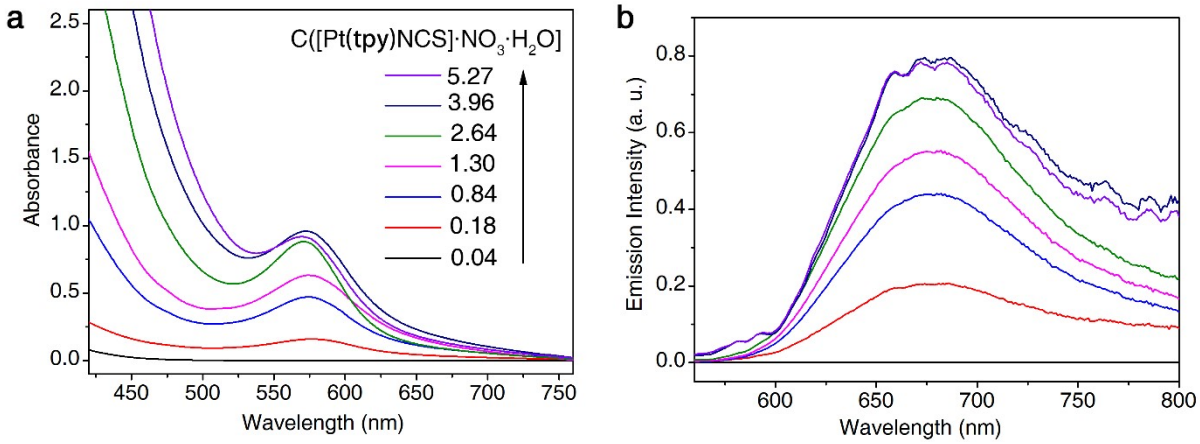

Fig. S11. a) UV-vis absorption changes by adding 0.2 mM perchlorate into [Pt(tpy)NCS]·NO_3·H_2O aqueous solution of different concentration. b) Corresponding emission spectra.

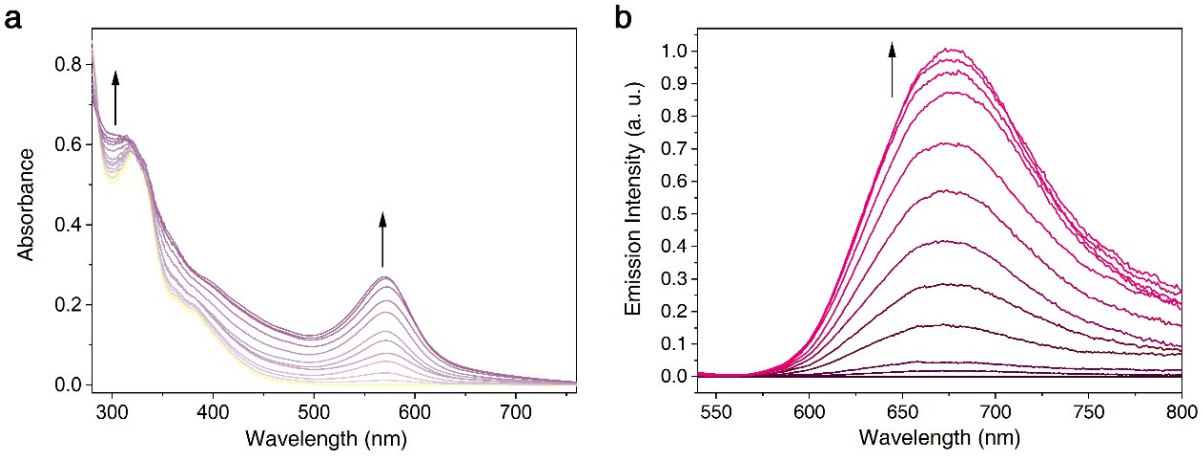

Fig. S12. a) UV-vis absorption changes of [Pt(tpy)NCS]·NO_3 aqueous solution (0.04 mM) with increasing chlorate content from 0 to 0.8 mM. b) Corresponding emission enhancement with increasing perchlorate content, excited at 527 nm.

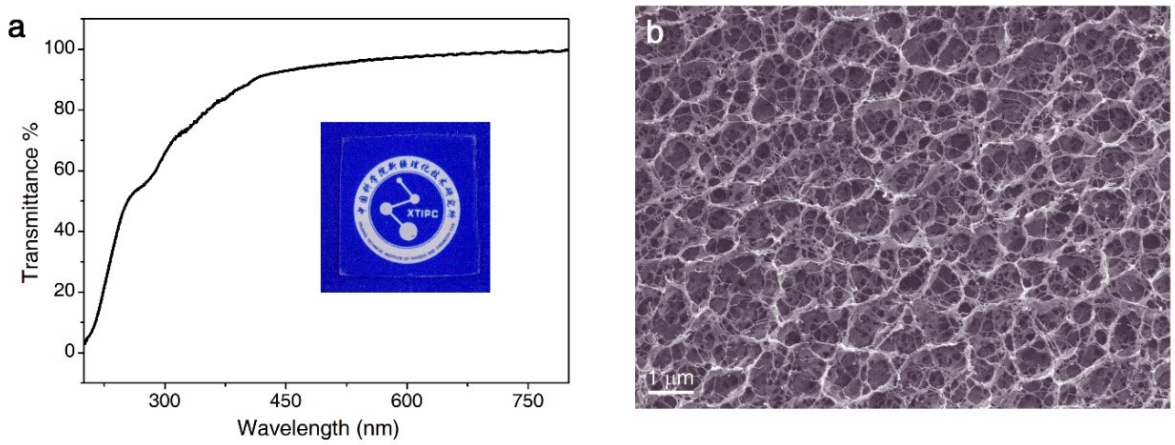

Fig. S13. a) SEM image of prepared PVA hydrogel. b) Optical transmittance of prepared PVA hydrogel (polymer concentration is 0.15 g/mL, 1 mm thick). Inset: The corresponding photograph.

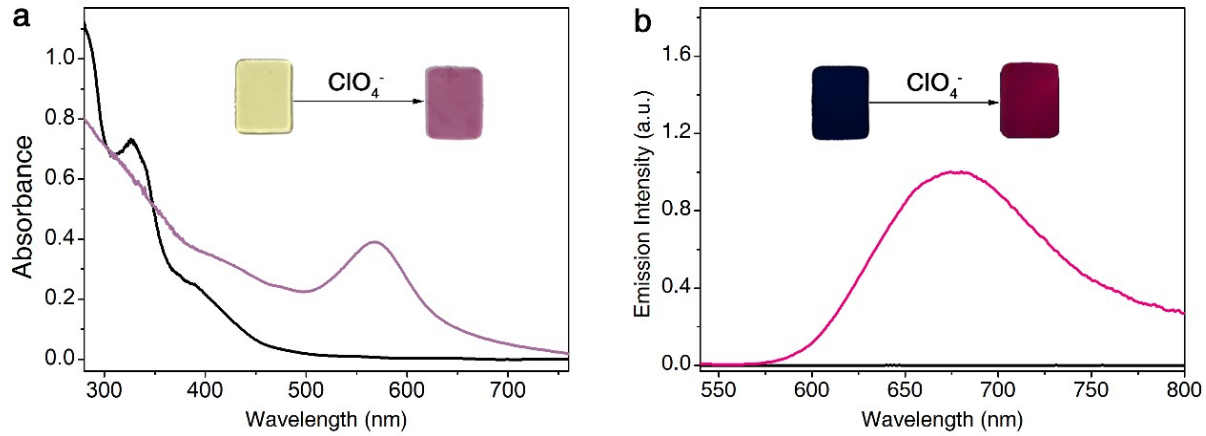

Fig. S14. a) UV-vis absorption spectra of [Pt(tpy)NCS]-PVA before and after reacting with ClO_4^- in aqueous solution. Inset: The corresponding photographs under sunlight. b) Emission spectra of [Pt(tpy)NCS]-PVA before and after reacting with ClO_4^- in aqueous solution. Inset: The corresponding photographs under 365 nm UV light.

Supplementary Tables

Table S1. Crystal data and structure refinement for $[Pt(tpy)NCS]\cdot NO_3\cdot H_2O$.

Compound	$[Pt(tpy)NCS]\cdot NO_3\cdot H_2O$
Empirical formula	$C_{16}H_{11}N_5SO_3Pt\cdot H_2O$
Formula weight	566.46
Temperature/K	100.00(10)
Crystal system	triclinic
Space group	P-1
a/Å	7.3640(4)
b/Å	11.3278(8)
c/Å	11.7118(10)
α/°	111.899(7)
β/°	106.700(6)
γ/°	97.274(5)
Volume/Å^3	837.67(11)
Z	2
ρ_{calc}g/cm^3	2.246
μ/mm^{-1}	8.536
F(000)	540.0
Crystal size/mm^3	0.11 × 0.1 × 0.08
Radiation	MoKα (λ = 0.71073)
2Θ range for data collection/°	4.016 to 49.998
Index ranges	$-8 \le h \le 8$, $-13 \le k \le 13$, $-13 \le l \le 13$
Reflections collected	9179
Independent reflections	2952 [R_{int} = 0.0587, R_{sigma} = 0.0635]
Data/restraints/parameters	2952/0/247
Goodness-of-fit on F^2	1.038
Final R indexes [I>=2σ (I)]	R_1 = 0.0345, wR_2 = 0.0759
Final R indexes [all data]	R_1 = 0.0390, wR_2 = 0.0795
Largest diff. peak/hole / e Å^{-3}	2.02/-2.17

The obtained single crystals have been deposited at the Cambridge Crystallographic Data Centre and allocated the deposition number: $[Pt(tpy)NCS]\cdot NO_3\cdot H_2O$ (1982814).

Table S2. Crystal data and structure refinement for $[Pt(tpy)L]\cdot ClO_4\cdot nH_2O$ (L = NCS^-, Cl^-, I^-; n = 0 or 1).

Compound	$[Pt(tpy)NCS]\cdot ClO_4\cdot H_2O$	$[Pt(tpy)Cl]\cdot ClO_4\cdot H_2O$[a]	$[Pt(tpy)I]\cdot ClO_4$
Empirical formula	$C_{16}H_{11}N_4SClO_4Pt\cdot H_2O$	$C_{15}H_{11}N_3Cl_2O_4Pt\cdot H_2O$	$C_{15}H_{11}N_3IClO_4Pt$
Formula weight	601.89	581.27	654.71
Temperature/K	100.00(10)	150(2)	100.00(11)
Crystal system	monoclinic	triclinic	triclinic
Space group	Cc	P-1	P-1
a/Å	12.3564	6.6281	6.9145
b/Å	12.3564	10.2133	10.908
c/Å	6.5138	13.3506	13.387
α/°	96.7355	104.376	110.985
β/°	96.7355	103.628	101.473
γ/°	115.439	90.548	94.8810
Volume/$Å^3$	876.181	848.59	910.305
Z	2	2	2
$\rho_{calc}g/cm^3$	2.281	2.275	2.389
μ/mm^{-1}	17.866	18.684	29.317
F(000)	1144.0	552	604.0
Crystal size/mm^3	0.12 × 0.1 × 0.08	0.18 × 0.03 × 0.02	0.12 × 0.11 × 0.1
Radiation	CuKα (λ = 1.54184)	-	CuKα (λ = 1.54184)
2 range for data collection/°	8.066 to 147.632	3.53 to 67.47	7.298 to 147.23
Index ranges	-16 ≤ h ≤ 16, -23 ≤ k ≤ 25, -4 ≤ l ≤ 7	-7 ≤ h ≤ , -12 ≤ k ≤ 11, -15 ≤ l ≤ 15	-8 ≤ h ≤ 4, -13 ≤ k ≤ 13, -15 ≤ l ≤ 16
Reflections collected	3325	6610	5874
Independent reflections	2055 [R_{int} = 0.0359, R_{sigma} = 0.0464]	2853 [R_{int} = 0.0335]	3550 [R_{int} = 0.0840, R_{sigma} = 0.1138]
Data/restraints/parameters	2055/77/253	2853/0/235	3550/39/226
Goodness-of-fit on F^2	1.049	1.011	1.021
Final R indexes [I>=2σ (I)]	R_1 = 0.0402, wR_2 = 0.1039	R_1 = 0.0348, wR_2 = 0.0821	R_1 = 0.0837, wR_2 = 0.1898
Final R indexes [all data]	R_1 = 0.0412, wR_2 = 0.1055	R_1 = 0.0401, wR_2 = 0.0843	R_1 = 0.1033, wR_2 = 0.2243
Largest diff. peak/hole / e $Å^{-3}$	2.89/-3.04	1.939/-1.109	2.46/-2.10

[a] Its crystal data was obtained from previous study.[2]

The obtained single crystals have been deposited at the Cambridge Crystallographic Data Centre and allocated the deposition number: $[Pt(tpy)NCS]\cdot ClO_4\cdot H_2O$ (1982809) and $[Pt(tpy)I]\cdot ClO_4$ (1982810).

Table S3. Photophysical data of $[Pt(terpy)L]\cdot ClO_4\cdot nH_2O$ (L = NCS, Cl and I, n = 0 or 1) in solid state.

Complex	Medium (T/K)	$\lambda(Absorb)_{max}$/nm	λ(Emiss)/nm (λ_{Ex}/nm)	Emission lifetime, τ (μs)	Luminescence quantum yield (%)
$[Pt(terpy)NCS]ClO_4\cdot H_2O$	Solid (298)	577	677 (295-520)	15.32	7.78
$[Pt(terpy)Cl]ClO_4\cdot H_2O$	Solid (298)	535	658 (295-520)	14.20	23.60
$[Pt(terpy)I]ClO_4$	Solid (298)	482	596 (295-520)	6.06	0.91

Table S4. Comparison of the experimental and computational results of the structure parameters of $[Pt(tpy)L]\cdot ClO_4\cdot nH_2O$ (L = NCS^-, Cl^- and I^-; n = 0 or 1).

Compound	Parameters	Experiment	DFT-D3	DFT-D3-BJ	VDW-without
$[Pt(tpy)NCS]\cdot ClO_4\cdot H_2O$	a (Å)	12.36	12.36	12.36	12.56
	b (Å)	12.36	12.36	12.36	12.56
	c (Å)	6.51	6.56	6.49	7.30
	alpha	96.74	96.60	96.60	96.53
	beta	96.74	96.60	96.60	96.53
	gamma	115.44	115.73	115.70	115.56
	Volume ($Å^3$)	876.18	881.85	872.89	1015.40
	Pt-Pt I length (Å)	3.27	3.29	3.26	3.65
	Pt-Pt II length (Å)	3.27	3.29	3.26	3.65
$[Pt(tpy)Cl]\cdot ClO_4\cdot H_2O$	a (Å)	6.67	6.63	6.58	7.16
	b (Å)	10.24	10.15	10.15	10.33
	c (Å)	13.39	13.34	13.33	13.71
	alpha	103.82	103.48	103.46	104.25
	beta	102.81	104.18	103.15	100.98
	gamma	90.49	91.27	91.05	90.74
	Volume ($Å^3$)	864.14	843.77	840.67	962.66
	Pt-Pt I length (Å)	3.33	3.29	3.28	3.59
	Pt-Pt II length (Å)	3.38	3.37	3.33	3.61
$[Pt(tpy)I]\cdot ClO_4\cdot H_2O$	a (Å)	6.91	7.12	7.06	7.77
	b (Å)	10.91	10.93	10.90	11.15
	c (Å)	13.39	13.33	13.33	13.56
	alpha	110.99	112.54	112.36	112.27
	beta	101.47	102.50	102.71	101.58
	gamma	94.88	97.43	97.25	93.46
	Volume ($Å^3$)	910.31	908.80	901.70	1052.55
	Pt-Pt I length (Å)	3.44	3.60	3.49	3.89
	Pt-Pt II length (Å)	3.67	3.95	3.64	4.08

Each crystal supercell consists of two identical molecules, but their positions of the two layers within the crystal are not equivalent. The shorter Pt-Pt distance is called “Pt-Pt I”, while the longer one is called “Pt-Pt II”. For each complex, three simulation schemes including DFT-D3 dispersion correction (DFT-D3), DFT-D3 with Becke-Johnson damping (DFT-D3-BJ), and simulation without dispersion correction (VDW-without) were performed to find the best scheme consisting with the experiment.

As is shown in Table S4, the structure parameters calculated without dispersion correction are quite different from those of the experiments. In all three types of crystals, the volume of primitive cell has an error of more than 10 %. When the dispersion correction is used in the calculation, the corresponding computational results have been greatly improved, and the error between the simulation results and the experimental results can be reduced to less than 1 %. This fact indicates that the non-covalent interactions of π-π stacking interaction and hydrogen bonding interaction actually play a key role in the crystal formation process. Further comparing the results of DFT-D3 and DFT-D3-BJ schemes, most of them are not much different except the Pt-Pt distance is better with the DFT-D3-BJ scheme in accordance with the experimental results. As the electrical structure of the layered crystals is quite sensitive to Pt-Pt distance, we believe that the calculation method with DFT-D3-BJ is more reliable in exploring the electrical property of the studied crystals. In order to maintain consistency, DFT-D3-BJ method has been used both in calculating electronic structure and optical properties of the different complexes.

Table S5. Calculation on the through-water binding energy of $[Pt(tpy)L]^+$ (L = NCS^- and Cl^-) to ClO_4^-.

L	E_L	E_{L-H_2O}	E_{H_2O}	E_f
NCS^-	-537.2955	-507.4565	-14.2435	-0.66
Cl^-	-499.3235	-470.8447	-14.2435	0.0041

Both the complex $[Pt(tpy)NCS]\cdot ClO_4\cdot H_2O$ and $[Pt(tpy)Cl]\cdot ClO_4\cdot H_2O$ contain two water molecules in the experimental structure. The binding energy E_f is defined as:

$$E_f = \frac{1}{2}[E_L - (E_{L-H_2O} + 2E_{H_2O})], \quad (1)$$

where E_L is total energy of the dehydrated form $[Pt(tpy)L]\cdot ClO_4$, E_{L-H_2O} is total energy of the hydrated form $[Pt(tpy)L]\cdot ClO_4\cdot H_2O$, E_{H_2O} is the total energy of water molecules. The calculation parameters are the same to the above parameters and a damped dispersion correction is implemented as well. In the calculation of E_{H_2O}, the 20 Å×20 Å×20 Å cubic cell is selected to ensure the accuracy of the calculations.

Table S6. Comparison of the computational results of the structure parameters of the hydrated form $[Pt(tpy)L]\cdot ClO_4\cdot H_2O$ and dehydrated form $[Pt(tpy)L]\cdot ClO_4$ ($L = NCS^-$ and Cl^-) by DFT-D3-BJ method.

Parameters	$[Pt(tpy)NCS]\cdot ClO_4$	$[Pt(tpy)NCS]\cdot ClO_4\cdot H_2O$
a (Å)	12.18	12.36
b (Å)	12.18	12.36
c (Å)	6.51	6.49
alpha	97.47	96.60
beta	97.47	96.60
gamma	115.34	115.70
Volume ($Å^3$)	847.27	872.89
Pt-Pt I length (Å)	3.26	3.26
Pt-Pt II length (Å)	3.26	3.26
	$[Pt(tpy)Cl]\cdot ClO_4$	$[Pt(tpy)Cl]\cdot ClO_4\cdot H_2O$
a (Å)	7.17	6.58
b (Å)	16.59	10.15
c (Å)	26.78	13.33
alpha	90.00	103.46
beta	91.89	103.15
gamma	90.00	91.05
Volume ($Å^3$)	3182.22	840.67
Pt-Pt I length (Å)	3.32	3.28
Pt-Pt II length (Å)	4.43	3.33

Table S7. Comparison of [Pt(tpy)NCS]-PVA hydrogel sensing platform with other methods.

Detection method (Readout mode)	Material	Cost	Onsite detection	Response rate	Pre-treatment	Detection limit for perchlorate		Ref.
						Solution	Solid	
Fluorescence (Single-mode)	Perylenediimide	Cheap	Yes	Fast	No	6×10^{-8} M	-	3
Fluorescence (Dual-mode)	Rhodamine	Cheap	Yes	Fast	No	1×10^{-7} M	-	4
Bioassay (Single-mode)	Perchlorate reductase	Cheap	Yes	Slow	No	2×10^{-8} M	-	5
Fluorescence (Single-mode)	Coordination polymer	Cheap	Yes	Fast	No	1.7×10^{-7} M	-	6
Fluorescence (Single-mode)	Tetraphenylethene -based compound	Cheap	Yes	Fast	No	3.8×10^{-7} M	-	7
Luminescence (Single-mode)	Ir(III) complex	Cheap	Yes	Fast	No	5×10^{-7} M	-	8
Inductively coupled plasma mass spectrometry (Single-mode)	-	Expensive	No	Medium	Yes	0.3×10^{-8} M	-	9
Capillary electrophoresis (Single-mode)	-	Expensive	No	Slow	Yes	1.8×10^{-7} M	-	10
Surface-enhanced Raman spectroscopy (Single-mode)	Diethyldithiocarbamate-modified Ag nanowire membrane	Expensive	No	Medium	Yes	-	2.0×10^{-9} g	11
Ion mobility spectrometry (Single-mode)	-	Expensive	Yes	Fast	Yes	-	6.3×10^{-9} g	12
Electrospray ionization mass spectrometry (Single-mode)	-	Expensive	No	Medium	Yes	-	1.0×10^{-10} g	13
Colorimetry and luminescence (Dual-mode)	[Pt(tpy)NCS]-PVA hydrogel	Cheap	Yes	Fast	No	1.4×10^{-8} M	2×10^{-17} g	This work

References

1. S. D. Taylor, A. E. Norton, R. T. Hart, Jr., M. K. Abdolmaleki, J. A. Krause and W. B. Connick, *Chem. Commun.*, 2013, **49**, 9161.
2. S. D. Taylor, W. Howard, N. Kaval, R. Hart, J. A. Krause and W. B. Connick, *Chem. Commun.*, 2010, **46**, 1070.
3. P. Singh, L. S. Mittal, V. Vanita, R. Kumar, G. Bhargava, A. Walia and S. Kumar, *Chem. Commun.*, 2014, **50**, 13994.
4. A. Sahana, A. Banerjee, S. Lohar, A. Chottapadhyay, S. K. Mukhopadhyay and D. Das, *RSC Advances*, 2013, **3**, 14044.

5. M. Heinnickel, S. C. Smith, J. Koo, S. M. O'Connor and J. D. Coates, *Environ. Sci. Technol.*, 2011, **45**, 2958-2964.
6. X. Zheng, R. Fan, K. Xing, K. Zhu, P. Wang and Y. Yang, *Chem. Eng. J.*, 2020, **380**.
7. N. Li, Y. Y. Liu, Y. Li, J. B. Zhuang, R. R. Cui, Q. Gong, N. Zhao and B. Z. Tang, *ACS Appl. Mater. Interfaces* 2018, **10**, 24249-24257.
8. G. Li, W. Guan, S. Du, D. Zhu, G. Shan, X. Zhu, L. Yan, Z. Su, M. R. Bryce and A. P. Monkman, *Chem. Commun.*, 2015, **51**, 16924-16927.
9. B. Lajin and W. Goessler, *Anal. Chim. Acta*, 2020, **1094**, 11-17.
10. M. L. Tan, M. Zhang, F. Li, F. Maya and M. C. Breadmore, *J. Chromatogr. A*, 2019, **1595**, 215-220.
11. Y.-e. Shi, W. Wang and J. Zhan, *Nano Res.*, 2016, **9**, 2487-2497.
12. L. Peng, L. Hua, W. Wang, Q. Zhou and H. Li, *Sci. Rep.*, 2014, **4**.
13. R. J. Soukup-Hein, J. W. Remsburg, P. K. Dasgupta and D. W. Armstrong, *Anal. Chem.*, 2007, **79**, 7346-7352.